

Synthesis, characterization, anti-proliferative activity and chemistry computation of DFT theoretical methods of hydrazine-based Schiff bases derived from methyl acetoacetate and α -hydroxyacetophenone

Sakineh Parvarinezhad, Mehdi Salehi*

Department of Chemistry, College of Science, Semnan University, P.O. Box 35195-363, Semnan, Iran

ARTICLE INFO

Article history:

Received 1 March 2020

Revised 1 August 2020

Accepted 13 August 2020

Available online 14 August 2020

Keywords:

Crystal structure

Schiff base, Ligand

2, 4-Dinitrophenylhydrazine

DFT calculation

MTT assay

ABSTRACT

In this study, the synthesized hydrazine Schiff bases belonging to methyl acetoacetate (**1**) and α -hydroxyacetophenone (**2**) were prepared by simple methods. In addition, FT-IR, UV-Vis, ^1H NMR, Mass spectra, along with melting point and conductivity measurements were used for the characterization of these compounds. The molecular structures of (**1**) and (**2**) were determined by single crystal X-ray diffraction technique. X-ray diffraction analysis reveals that (**1**) crystallizes in the orthorhombic system with $Pca2_1$ space group possessing $a = 21.1032(12)$, $b = 5.9061(3)$, $c = 10.9717(7)$, $\beta = 90^\circ$ while compound (**2**) crystallizes in the monoclinic system with $P2_1/c$ space group and $a = 7.0386(14)$, $b = 13.275(3)$, $c = 15.071(3)$, $\beta = 99.27(3)^\circ$. Also, theoretical studies were performed within the density functional theory (DFT) framework. Hydrazine compounds (**1**) and (**2**) were geometrically optimized using the B3LYP method with (6-311+G+ (d, p)) basis set. Calculated geometrical parameters exhibited a good agreement with experimental value. The optimized parameters from the DFT calculations were in line with experimentally measured Single Crystal X-ray Diffraction (SCXRD) results. The anticancer effects of the synthesized compounds were assayed using MTT assay against cancer cell lines K562 and MG63.

© 2020 Elsevier B.V. All rights reserved.

1 Introduction

Schiff bases have been considered as privileged ligands in coordination chemistry due to their simple preparation methods, diversity, and structural variability [1]. Moreover, the Schiff bases and their complexes have been widely studied in various fields including catalysis [2], material science [3], optoelectronic applications [4], medicinal chemistry [5], radiopharmaceuticals [6]. In this regard, finding an alternative approach to enhance drug stability by changing the structural properties of these compounds sounds crucial. On the other hand, hydrazones, which can form an azomethine imine, are a major class of reagents in organic synthesis due to their advantages such as accessibility, stability, and different structure-dependent reactivity, and reaction conditions [7, 8]. Hydrazine Schiff bases are also a proper candidate in physiological and biological studies due to their antimycobacterial, antitumor, cytotoxic, antiviral, and properties, they have also found extensive applications in materials science [9–12]. These activities are attributed to their crystallographic features as they form stable chelate compounds with transition metals which can catalyze

physiological activities [13–19]. Due to their importance in biological processes, the hydrazines can serve as linkers for drug release to enhance the therapeutic effects against cancer and decrease the side effects [20]. The design, synthesis, characterization, and structures of various hydrazine-based Schiff bases have been studied. These structures will certainly deliver useful information about their coordination properties [21–25]. In the present study, two Schiff base compounds were synthesized from hydrazine derivatives with different ketones (Scheme 1). Their characteristics were investigated through different physical and chemical methods. Furthermore, DFT structural calculations as well as cytotoxicity assessment towards cancer cell line of K562 and MG63 were discussed.

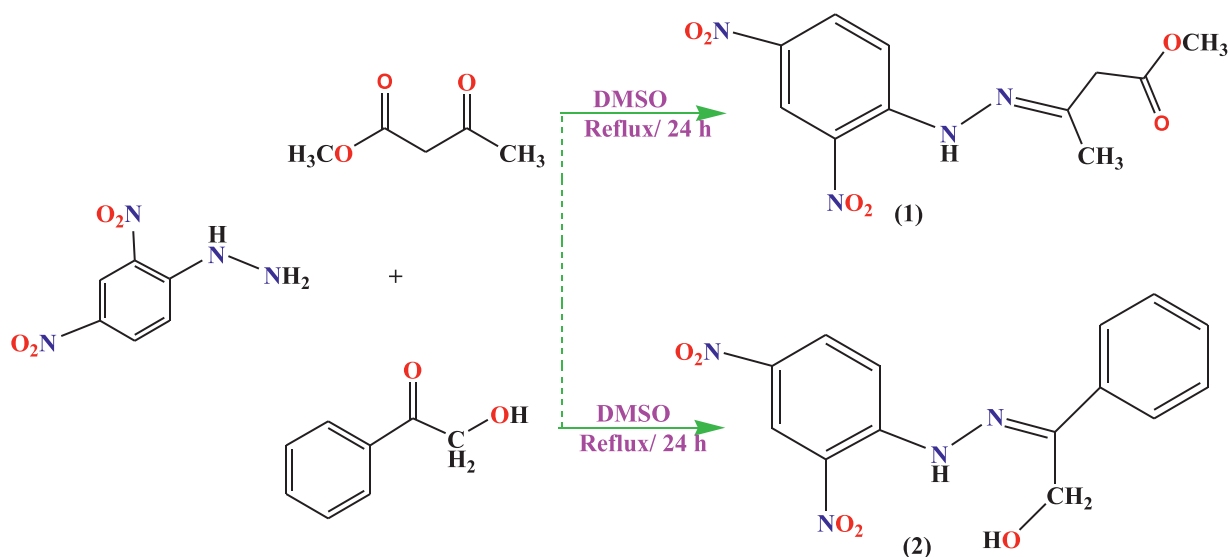
2. Experimental

2.1. Materials and physical measurements

All the chemicals and solvents were purchased from Aldrich and Merck. A SHIMADZU UV-1650 PC spectrophotometer was used for UV-Vis spectroscopy in ethanol. The FT-IR spectra were recorded on FT-IR SHIMADZU spectrophotometer using KBr pellets at room temperature in the wavenumber range of $4000\text{--}400\text{ cm}^{-1}$. The melting point was determined in open capillaries on an elec-

* Corresponding author.

E-mail address: msalehi@semnan.ac.ir (M. Salehi).



Scheme 1. Synthetic procedure for the preparation of hydrazine-based Schiff Bases (1) and (2).

trothermal 9100 apparatus. The molar conductivity values of the solutions fell within the range observed for 1:1 electrolytes [26]. ^1H NMR spectra at room temperature was recorded in $\text{DMSO-}d_6$ using Varian - INOVA 500 MHz NMR spectrophotometer. The Mass spectra was recorded on Agilent Technology (HP) 5973 Network Mass Selective Detector. All theoretical studies were accomplished using density functional theory (DFT) in the Gaussian 09 program software. Cell lines were obtained from Pasteur Institute of Iran (Tehran, Iran) and cell culture medium (RPMI 1640), fetal bovine serum (FBS) and penicillin-streptomycin were purchased from Gibco BRL (Life technologies, Paisley, Scotland). The culture plates were obtained from Nunc (Roskilde, Denmark). MTT [3-(4, 5'-dimethylthiazol-2-yl)-2, 5-diphenyltetrazolium bromide] was purchased from Sigma. Chem. Co. (Munich, Germany).

2.2. Synthesis of compounds (1) and (2)

2.2.1. General synthesis

The Schiff bases were synthesized through a general procedure. Compounds (1) and (2) were prepared by the reaction of 2, 4-dinitrophenylhydrazin (0.99 g, 0.5 mmol) with methyl acetoacetate (0.058 g, 0.5 mmol) / α - hydroxyacetophenone (0.068 g, 0.5 mmol) in DMSO (10 mL). The mixtures were then refluxed for 24 h. After some days at room temperature, orange crystals were collected by filtration, washed with a small amount of diethyl ether and dried under pressure.

2.2.2. Compound (1)

Methyl (Z)-3-(2-(2, 4-dinitrophenyl)hydrazono)butanoate (1) Orange crystals. Yield: 70%. Mol.Wt: 295.24 g/mol. M. p.: 166. ΔM (DMSO) = $5.88 \mu\text{scm}^{-1}$. FT-IR: (KBr, cm^{-1}): 3125($\nu_{\text{N-H}}$), 3118 ($\nu_{\text{C-H}}$), 3095 (ν_{Methyle}), 1613($\nu_{\text{C=N}}$), 1405, 1339(ν_{NO_2}), 1055($\nu_{\text{HN-N}}$). UV-Vis: λ_{max} (nm) (ϵ , $\text{M}^{-1} \text{cm}^{-1}$) (EtOH): 249(30, 000), 390(46, 500), 432(43, 000).

2.2.3. Compound (2)

(Z)-3-(2-(2, 4-dinitrophenyl)hydrazono)-3-phenylpropan-1-ol (2) Orange crystals. Yield: 85%. Mol.Wt: 316.28 g/mol. M. p.: 188. ΔM (DMSO) = $5.88 \mu\text{scm}^{-1}$. FT-IR: (KBr, cm^{-1}): 3260($\nu_{\text{O-H}}$), 3115($\nu_{\text{N-H}}$), 2984, 2489($\nu_{\text{C-H}}$) 1614($\nu_{\text{C=N}}$), 1525, 1446 (ν_{NO_2}), 1069($\nu_{\text{HN-N}}$). UV-Vis: λ_{max} (nm) (ϵ , $\text{M}^{-1} \text{cm}^{-1}$) (EtOH): 243(350, 000), 295(16, 300), 385(66, 300).

2.3. Crystal structure determination

Diffraction data were collected by the ω -scan technique, using graphite-monochromated $\text{MoK}\alpha$ radiation ($\lambda = 0.71073 \text{ \AA}$), at 200 K (1) on Rigaku XCalibur four-circle diffractometer with EOS CCD detector and at room temperature (2) on MAR345 dtb four-circle diffractometer with MAR345 image plate detector. The data were corrected for Lorentz-polarization as well as for absorption effects [27]. Precise unit-cell parameters were determined by a least-squares fit of the reflections of the highest intensity, chosen from the whole experiment. The structures were solved with SHELXT-2013 [28] and refined with the full-matrix least-squares procedure on F^2 by SHELXL-2013 [28]. All non-hydrogen atoms were refined anisotropically, all hydrogen atoms were placed in idealized positions and refined as 'riding model' with isotropic displacement parameters set at 1.2 (1.5 for CH_3) times U_{eq} of appropriate carrier atoms. The crystals of (2) were of low quality, therefore the diffraction data allowed only for determination of the structure, but the R factors etc. are relatively high. Nevertheless, the geometry of molecule as well as intermolecular interactions can be reliably determined. Table 1 shows the crystallographic data. Crystallographic data for the structural analysis has been deposited with the Cambridge Crystallographic Data Centre, Nos. CCDC - 1908139 - 1908141. Copies of this information may be obtained free of charge from: The Director, CCDC, 12 Union Road, Cambridge, CB2 1EZ, UK; e-mail: deposit@ccdc.cam.ac.uk, or www: www.ccdc.cam.ac.uk.

2.4. Computational details

The compounds (1) and (2) were theoretically studied (DFT) and their atomic orbitals were examined to elucidate the chemical phenomena and changes in the molecules. Theoretical studies were conducted within density functional theory (DFT) framework using B3LYP hybrid functional proposed by Becke [29, 30] and Lee, Yang and Parr [31] and 6-311+G (d, p) basis set to geometrically optimize the compounds (1 and 2) [32, 33]. Gaussview 5.0 was applied to prepare the input files, while Gaussian09 software was utilized for all the geometry optimization calculations at the B3LYP level of theory [33]. The structures of the compounds were fully optimized with no constraint. The frequency calculations were also carried out on the optimized structures to confirm that the optimized structures are real local minima on the potential energy

Table 1
Crystal data, data collection and structure refinement.

Compound	(1)	(2)
Formula	C ₁₁ H ₁₂ N ₄ O ₆	C ₁₄ H ₁₂ N ₄ O ₅
Formula weight	295.24	316.28
Crystal system	Orthorhombic	Monoclinic
Space group	Pca2 ₁	P2 ₁ /c
a(Å)	21.1032(12)	7.0386(14)
b(Å)	5.9061(3)	13.275(3)
c(Å)	10.9717(7)	15.071(3)
β(°)	90	99.27(3)
V(Å ³)	1367.49(14)	1389.8(5)
Z	4	4
D _x (g cm ⁻³)	1.434	1.512
F(000)	612	656
μ(mm ⁻¹)	0.119	0.118
Reflections:		
Collected	7277	8461
unique (R _{int})	2707 (0.029)	2395 (0.135)
with I > 2σ(I)	1867	1670
R(F) [I > 2σ(I)]	0.051	0.124
wR(F ²) [I > 2σ(I)]	0.123	0.302
R(F) [all data]	0.081	0.163
wR(F ²) [all data]	0.143	0.323
Goodness of fit	1.03	1.12
max/min Δρ (e·Å ⁻³)	0.27/-0.22	0.34/-0.29

surfaces. UV-Vis spectra and electronic transitions were computed with the time-dependent DFT (TD-DFT) method at the B3LYP/ (6-311 + G (d, p)) level.

2.5. Biological studies

2.5.1. Cell culture

Cells were cultured in the RPMI medium (RPMI1640, Sigma). The medium was supplemented with 10% heat-inactivated fetal calf serum (Sigma) and streptomycin (10 mg/mL)-penicillin (5 μg/mL) was utilized as antibiotics at 37 °C under a humidified atmosphere containing 5% CO₂. The cells should have 80–90% confluence before they are harvested and plated for the experiments.

2.5.2. Assessment of cytotoxicity using MTT assay

The cell proliferation of 2, 4-dinitrophenylhydrazine, compounds (1), (2), and 5-fluorouracil were determined in K562 (myelogenous leukemia cancer) and MG63 (osteosarcoma cancer) cell lines through the MTT assay. The harvested cells with a density of 1 × 10³ cells/well were seeded in 96-well plates and cultured for 24 h. Three replica wells were used for all concentrations and control overnight. Then the media were removed and various amounts of compounds (1) and (2) (2, 2.5, 5, 10, 15, 20, and 25 ng/mL) were added to the wells. The plates were incubated in a humidified atmosphere 5% CO₂ for 48 h. After treatments of the compounds, 20 μL of MTT Formosan precipitate (5 mg/mL) was added to each well and incubated for an additional 4 h. Then, the culture medium of the plate was removed and 100 μL of DMSO was added to dissolve the MTT Formosan precipitate. The absorbance of samples in each well was determined at 570 nm.

3. Results and discussion

3.1. Synthesis

Two new compounds were synthesized via reacting 2, 4-dinitrophenylhydrazine with methyl acetoacetate, and α-hydroxyacetophenone in DMSO. All compounds were soluble in organic solvents such as DMSO, MeOH, and EtOH. These compounds were characterized by FT-IR, UV-Vis, ¹H NMR, Mass spectra, melting point assessment, and conductivity measurement. The crystal

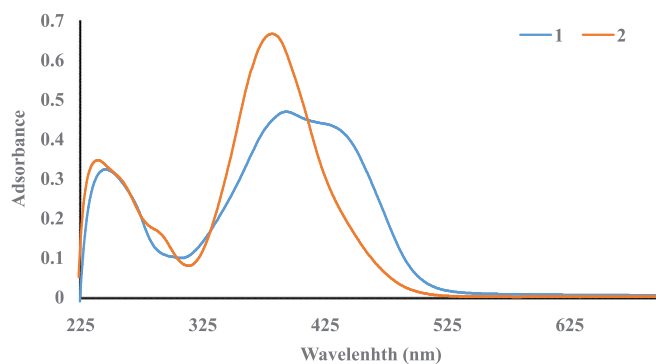


Fig. 1. UV-Vis spectrum of compounds (1) and (2) in EtOH solutions ($c = 10^{-5}$ M).

structures of the compounds were determined by Single-Crystal X-ray Diffraction (SCXRD)

3.2. Spectroscopic characterization of the compounds (1) and (2)

Several spectroscopic methods have been used to confirm the synthesis of the compounds (1) and (2). FT-IR spectra can offer sufficient information to clarify the bonding status of the compounds. The FT-IR spectra of the Schiff base compounds are presented in Figures S.1 and S.2 (Supplementary materials). FT-IR spectrum of methyl acetoacetate exhibited two signals at around 1652 and 1631 cm⁻¹ which can be assigned to the stretching vibrations of the C=O groups. Upon the formation of the azomethine groups in the Schiff base Methyl(Z)-3-(2-(2, 4-dinitrophenyl)hydrazono)butanoate (1), these bands disappeared and a new intense band emerged at 1613 cm⁻¹. This is the most characteristic band of the similar Schiff base ligands and is indicative of the formation of the C=N band. The band at 3125 cm⁻¹ can be attributed to the ν(N-H) stretching frequency for compound (1). Also, the band at 1055 cm⁻¹ indicates the HN-N vibration in the Schiff bases; another evidence for the successful synthesis of this compound. In the case of (2) α-hydroxyacetophenone, the signals at 1689 cm⁻¹ are assigned to the stretching vibrations of the C=O groups. Upon the formation of the azomethine groups in the Schiff base (Z)-3-(2-(2, 4-dinitrophenyl)hydrazono)-3-phenylpropan-1-ol (2), these band disappeared and a new intense one appeared at 1614 cm⁻¹. This band at 3260 cm⁻¹ can be assigned to stretching vibration of OH (ν_{OH}) in compound (2). The band at 3115 cm⁻¹ can be related to the ν(N-H) stretching frequency for compound (2) [8]. The band at 1069 cm⁻¹ can be also assigned to the HN-N vibration in the spectra of the Schiff base (2).

The UV-Vis spectra of the compounds (1), (2) are depicted in Figs. 1. The absorption spectra of the prepared compounds were recorded in EtOH (10⁻⁵ M). In the UV-Vis spectrum of the Schiff base compound (1), an intense peak at around 249 nm can be assigned to the π → π* transitions of the aromatic rings. The shoulder signal at 390 nm can be also attributed to the π → π* transitions of the azomethine groups while the peak at 432 nm is related to the n → π* transition.

In the electronic absorption spectra of the compound (2), an intense peak at around 243 nm is indicative of the π → π* transitions of the aromatic rings. The shoulder signal at 295 nm can be also assigned to the π → π* transitions of the azomethine groups. On the other hand, the π → π* transitions of the azomethine group showed a blue shift by about 95 nm. The peak at 385 nm can be also attributed to the π → π* transition in the (C=N), which blue-shifted by 47 nm compared to the compound (1) [25,34].

The synthesized compounds (1) and (2) were diamagnetic and hence, NMR spectroscopy provided useful characterization data. In the ¹H NMR spectrum of the Schiff base compound (1) Figures

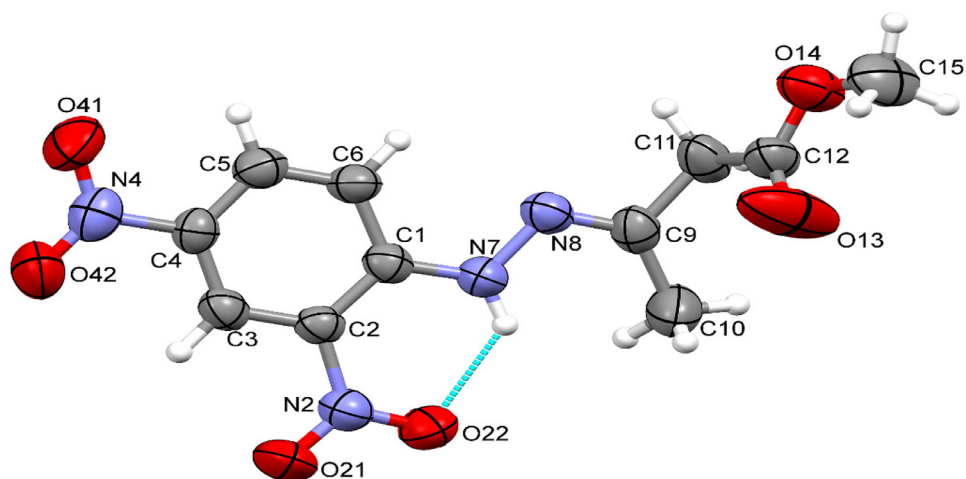


Fig. 2. ORTEP view of **1**, together with the numbering scheme. Ellipsoids are drawn at the 50% probability level; hydrogen atoms are represented by spheres of arbitrary radii. Intramolecular hydrogen bond is shown as dashed blue line. (For interpretation of the references to color in this figure legend, the reader is referred to the web version of this article.)

Table 2

Selected geometrical parameters (Å, °) with s.u.'s in parentheses. Capital letters denote the least-squares planes: A – nitrophenyl ring, B – nitro group at position 2, C – nitro group at 4, D – the C–N–N=C–C chain, and E – the terminal group: COOC (**1**) or phenyl ring (**2**).

	(1)				(2)			
N–O	1.218(5)	1.233(5)	1.222(5)	1.238(5)	1.232(7)	1.236(7)	1.225(8)	1.226(8)
C1–N7		1.356(5)				1.361(8)		
N7–N8		1.383(5)				1.371(7)		
N8–C9		1.282(5)				1.286(7)		
O–N–O		122.2(4)	123.5(4)			121.1(6)	120.9(7)	
C1–N7–N8		119.0(4)				118.1(5)		
N7–N8–C9		116.2(3)				118.5(5)		
A/B		4.1(5)				7.8(6)		
A/C		4.0(7)				4.9(4)		
B/C		5.6(8)				10.4(8)		
A/D		8.0(2)				1.36(17)		
D/E		68.8(3)				1.89(17)		
A/E		71.1(2)				1.83(16)		

S.3 (Supplementary materials), the signal above 10 ppm could be due to the protons of N–H groups (a). The multiplets at around 7–8 ppm could be assigned to the aromatic protons (b). Other signals were also consistent with the proposed structure and attributed to the experimental section. The signal above 3.5 ppm was due to the protons of O–CH₃ groups (c). The protons due to the CH₂ groups with appropriate intensity has also appeared at 3.4 ppm was consistent with the obtained structures (d). The signal above 2 ppm was due to the protons of CH₃ groups (e).

In the ¹H NMR spectrum of the Schiff base compound (**2**) Figures S.4 (Supplementary materials), the signal above 13 ppm was due to the protons of N–H groups (a). The multiplets at around 7–8 ppm were due to the aromatic protons (b). The signal 6.5 ppm was due to the protons of O–H groups (c). The protons due to the CH₂ groups with appropriate intensity has also appeared at above 4 ppm was consistent with the obtained structures (d) [35]. The Mass spectrum of Schiff base compounds, (**1**) and (**2**) Figures S.5, 6 (Supplementary materials) showed a molecular ion peak [M]⁺ at *m/z* 296, 316 which corresponds to its proposed molecular formula, respectively.

3.3. Description of the crystal structures

ORTEP views of the molecules are shown in Figs. 2 and 3 selected geometrical parameters are listed in Table 2. The conformation of the molecules can be described by dihedral angles between

Table 3

Hydrogen bond data for ligands (**1**) and (**2**) (Å, °).

D	H	O	D–H	H...O	D...O	D–H...O
(1)						
N7	H7	O22	0.86(5)	2.02(6)	2.617(5)	126(5)
(2)						
N7	H7	O22	0.86	2.00	2.617(7)	128
N7	H7	O11	0.86	2.18	2.785(8)	127

the approximately planar fragments (cf. Table 2). The nitro groups are almost slightly twisted with respect to the phenyl ring plane, as can be expected for non-neighbouring groups. Molecules (**2**) are in quite good approximation planar, while in molecule (**1**) due to the presence of methylene group the terminal ether fragment is relatively tilted. Table 3 show is Hydrogen bond data (Å, °).

As can be seen in Fig. 4, this is the only important difference between the molecules, the rest of the molecules are very similar. Intramolecular N–H...O hydrogen bonds (bifurcated in case of (**2**)) additionally add for the stability of planar conformation. In the crystal structures of (**2**) the principal role is played by $\pi \cdots \pi$ interactions, which connect molecules into dimers (interplanar distances around 2.4 Å), for which the UNI intermolecular potentials have by far the highest absolute values, around –100 kJ/mol [36, 37]. In (**1**), due to the presence of methylene groups such a good fit is not possible and therefore the highest potentials between

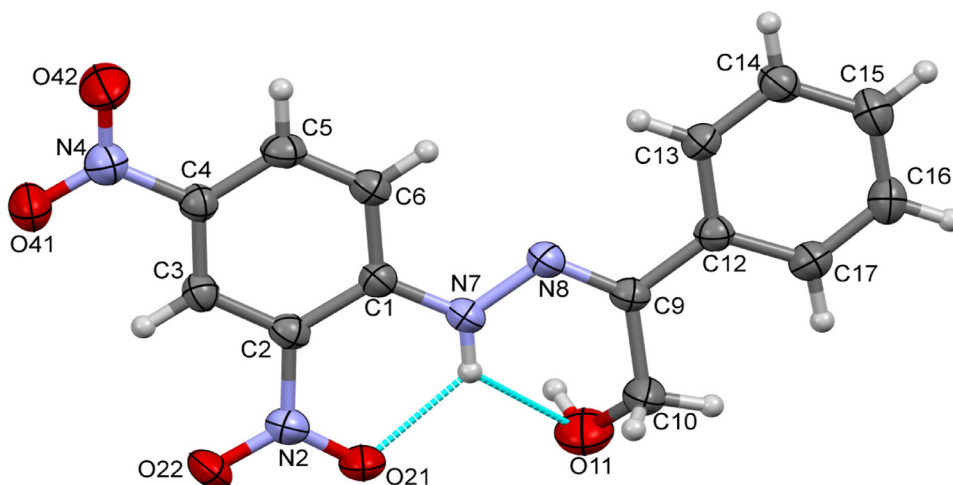


Fig. 3. ORTEP view of **2**, together with the numbering scheme. Ellipsoids are drawn at the 50% probability level; hydrogen atoms are represented by spheres of arbitrary radii. Intramolecular hydrogen bond is shown as dashed blue line. (For interpretation of the references to color in this figure legend, the reader is referred to the web version of this article.)

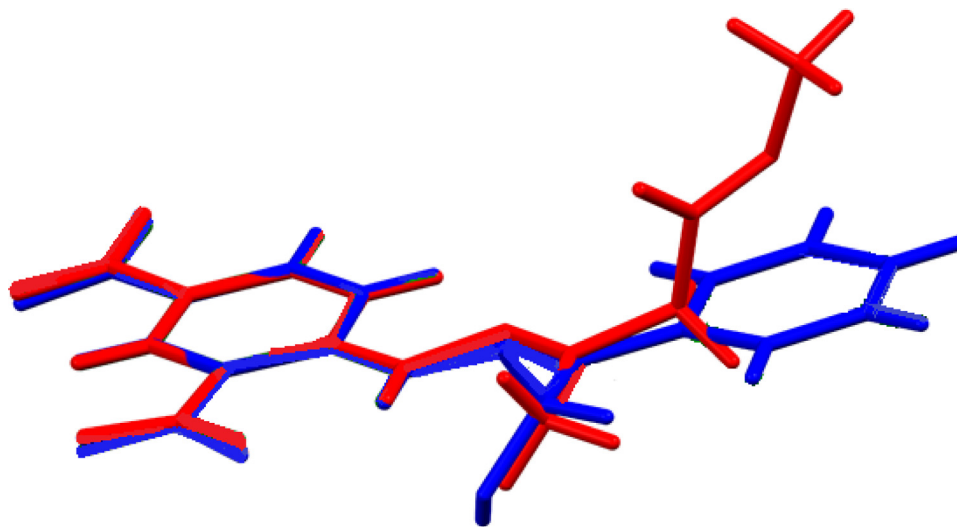


Fig. 4. A comparison of the shapes of molecules **1** (red) and **2** (blue). The nitrophenyl rings were fitted. (For interpretation of the references to color in this figure legend, the reader is referred to the web version of this article.)

neighbours are almost two times smaller. Interestingly, the potentials calculated for hydrogen-bonded pairs are even smaller, up to -20 kJ/mol.

3.4. Computational chemistry and density functional theory (DFT) calculations

3.4.1. Computational molecular structure

All the DFT calculations, including the full geometry optimizations for Methyl (*Z*)-3-(2-(2, 4-dinitrophenyl)hydrazono)butanoate (**1**) and (*Z*)-3-(2-(2, 4-dinitrophenyl)hydrazono)-3-phenylpropan-1-ol (**2**), were conducted using CIF as the experimental structure to obtain the vibrational frequency from the basis set (i.e., 6-311+G (d, p)). After optimizations, the geometric parameters of the computational data (e.g. bending angles, the torsional angles, and the bond lengths) were analyzed by Gaussview and compared with the experimental data. The comparison of data showed slightly computed larger bond length and angle as compared with the experimental data. According to [Table 4](#), the bond length and angles ob-

tained by B3LYP method for (**1**) and (**2**) compounds are more consistent with investigational information.

3.4.2. Vibrational analysis

Frequency calculations were performed at this level of theory which confirmed that the optimized structures belonged to the minima on the potential energy surface. Fig. S1 shows the experimental and calculated FT-IR spectra of compounds. [Table 5](#) lists the experimental vibrational wavenumbers and their corresponding calculated values with the probable assignments.

According to [Table 5](#), the B3LYP method was more consistent with the empirical data. The C–H stretching vibration modes of CH_2 occur in the range of $2984\text{--}3095\text{ cm}^{-1}$ in compounds (**2**) and (**1**), respectively. Meanwhile, the peaks in the range of $2977\text{--}3102\text{ cm}^{-1}$ (B3LYP/6-311+G (d, p)) can be attributed to the C–H stretching vibration modes. The stretching vibration modes of C–H bonds of phenyl ring occurred at 3118 and 2489 cm^{-1} in compounds (**1**) and (**2**), respectively; the B3LYP method showed the mentioned peaks at 3237 , 2977 cm^{-1} , respectively. The experimental N–H stretching vibration mode of compounds (**1**) and (**2**)

Table 4

The most important geometric parameter including the bond length (Å), the bond angles and the torsion angles (°) calculated in the base set 6-311+G(d, p).

Parameter	X-ray	B3LYP/6-311+G(d, p)
Length bond (1)		
C=N H- N-O(Ortho)N-O(Para) C-N C-O	1.282 0.860 1.222,1.238 1.218,1.233 1.356 1.170,1.296	1.284 1.016 1.225, 1.227 1.221, 1.242 1.360 1.206, 1.344
Angels		
H-N-N C=N- N-O(Ortho) N-O(Para)	118.71 116.20 122.24 123.54	122.80 117.24 122.97 124.71
Length bond (2)		
C=N	1.286	1.290
H-N	0.86	1.019
N-O(Ortho)	1.226,1.232	1.226,1.239
N-O(Para)	1.225,1.236	1.225,1.227
C-N	1.361	1.362
O-H	0.854	0.963
C-O	1.371	1.430
Angels		
H-N-N	139.97	120.85
C=N-N	118.15	118.12
N-O(Ortho)	121.16	123.16
N-O(Para)	120.91	124.68
C=N-N	118.55	118.12
N-O(Ortho)	121.18	123.16

Table 5

The important vibrational frequency of experimental and computational data and vibrational modes using the B3LYP and experimental data in the base set (6-311+G (d, p)).

Experimental	Calculated B3LYP/6-311+G (d, p)	Tentative assignment
(1)		
3125	3480	ν (N-H)
3118	3237	ν (C-H) _{Ph}
3095	3102	ν (C-H) _{CH₂}
3083	3163,3133,3054	ν (CH ₃) _{methoxy}
1678	1791	ν (C=O)
1613	1684	ν (C=N)
1405,1339	1594,1361	ν (NO ₂)
(2)		
3260	3830	ν (O-H)
3115	3436	ν (N-H)
2984	3085	ν (C-H) _{CH₂OH}
2489	2977	ν (C-H) _{Ph}
1614	1654,1648	ν (C=N)
1525,1446	1561,1359	ν (NO ₂)

can be observed at 3125 and 3115 cm⁻¹; theoretical investigation showed wavenumbers higher than about 3480, 3436 cm⁻¹ (for B3LYP method). The stretching vibration modes of C=N bonds are indexed to the bands at 1684, 1654–1648 (for B3LYP method) for compounds **(1)** and **(2)**. The results showed that computational chemistry could properly reproduce the structure of the compounds.

3.4.3. UV-Vis spectrum

TD-DFT calculations were also applied for a better description of the experimental UV-Vis signals. Using TD-DFT calculations, spectral characteristics such as maximum energy excitation, and oscillation strengths can be calculated. Hence, only the single transitions of absorption bands with oscillation strengths (>0.03) and wavelengths (>200) nm in the methanol, ethanol and DMSO solvents for compounds **(1)** and **(2)** are shown in Table 6. The UV-Vis spectrum of **(1)** in EtOH showed a band at 249 nm that may be assigned to the $\pi \rightarrow \pi^*$ transition in the aromatic ring. The results calculated in the same solvent indicated the absorption band at 256–266 nm with a bond energy of 4.826–4.657 eV

with oscillator strengths of 0.0329 - 0.0531 eV and at 390 nm which can be assigned to the $\pi \rightarrow \pi^*$ transition in C=N. The $\pi \rightarrow \pi^*$ transition in C=N in **(1)** was observed at around 369 nm with a bond energy of 3.355 eV and $f = 0.5730$ (orbital excitation: HOMO→LUMO +1, 97% contribution). The TD-DFT calculations also confirmed the existence of a signal in this region. The calculated wavelength is in good agreement with the experimental value. Also, the maximum absorption by the electronic transmissions of HOMO →LUMO occurred with the oscillation strength of 0.0899 and the band energy of 2.916 eV at a wavelength of 418 nm ($n \rightarrow \pi^*$ transition in C=N). The spectrum obtained from TD-DFT calculations in methanol showed the absorption band in the range of 256–266 nm with a bond energy of 4.825–4.654 eV and oscillator strengths of 0.0328–0.1057 the absorption band of 369 nm with a bond energy of 3.356 eV and with oscillator strengths of 0.5670. In the case of DMSO solvent, TD-DFT computations exhibited an absorption band at 257–273 nm with a bond energy of 4.822–4.531 eV and oscillator strengths of 0.0329–0.0472 as well as an absorption band at 371 nm with a bond energy of 3.339 eV and oscillator strength of 0.582. For **(2)**, The UV-Vis spectrum in EtOH showed a band at 243 nm which may be assigned to the $\pi \rightarrow \pi^*$ transition in the aromatic ring. The results calculated in the same solvent indicated an absorption band at 274 nm with a bond energy of 4.523 eV and oscillator strength of 0.0817. The band at 295 nm can be assigned to the $\pi \rightarrow \pi^*$ transition in C=N. The calculated results indicated an absorption band at 305 nm with a bond energy of 4.055 eV and $f = 0.2037$ (orbital excitation: HOMO→LUMO+2 65%, HOMO-2→LUMO+1 25%, HOMO-2→LUMO 5% and HOMO-1→LUMO+1 2%). Moreover, the maximum absorption by the electronic transmissions of HOMO →LUMO with the oscillation strength of 0.1238 and the energy of 2.653 eV was determined at 467 nm. The spectrum obtained from TD-DFT calculations in MeOH solvent exhibited an absorption band at 274 nm with a bond energy of 4.525 eV and $f = 0.0870$ and one at 305 nm with a bond energy of 4.055 eV and $f = 0.2046$. The spectrum obtained from calculations in DMSO showed two absorption bands; one at 274 nm with a bond energy of 4.159 eV and $f = 0.1231$ and the other at 306 nm with a bond energy of 4.048 eV and $f = 0.2058$. The calculated wavelength is in good agreement with the experimental data. Polar solvents can affect the geometric and electronic structure as well as the properties of the molecule

Table 6
Unique absorption bands with oscillation strengths (>0.03) and wavelength (>200) nm.

Solvent	λ_{cal}	f	Energy (eV)	Combining configuration with absorption coefficient (>0.2)	Assignment
(1)					
Methanol	256	0.0328	4.825	(66 ->78), 0.31365,	$(\pi \rightarrow \pi^*)_{aromatic\ ring}$
	266	0.1057	4.658	(73 ->78), 0.26661	$(\pi \rightarrow \pi^*)_{aromatic\ ring}$
	369	0.5670	3.356	(74 ->78), 0.37184,	$(\pi \rightarrow \pi^*)_{C=N}$
	418	0.0899	2.916	(74 ->79), 0.33232 (77 ->79), 0.69710 (77 ->78), 0.69806	$(n \rightarrow \pi^*)_{C=N}$
Ethanol	256	0.0329	4.826	(66 ->78), 0.30560,	$(\pi \rightarrow \pi^*)_{aromatic\ ring}$
	266	0.0531	4.657	(73 ->78), 0.28011	$(\pi \rightarrow \pi^*)_{aromatic\ ring}$
	369	0.5730	3.355	(74 ->79), 0.31916,	$(\pi \rightarrow \pi^*)_{C=N}$
	418	0.0913	2.962	(76 ->79), 0.42568 (77 ->79) 0.69761 (77 ->78) 0.69859	$(n \rightarrow \pi^*)_{C=N}$
DMSO	257	0.0329	4.822	(66 ->78), 0.32161,	$(\pi \rightarrow \pi^*)_{aromatic\ ring}$
	266	0.0527	4.650	(73 ->78), 0.25752	$(\pi \rightarrow \pi^*)_{aromatic\ ring}$
	371	0.582	3.339	(75 ->79) 0.45556,	$(\pi \rightarrow \pi^*)_{C=N}$
	420	0.0939	2.951	(76 ->79) 0.24338 (77 ->79) 0.69695 (77 ->78) 0.69789	$(n \rightarrow \pi^*)_{C=N}$
CH₂Cl₂	256	0.0292	4.829	(66 ->78), 0.20499,	$(\pi \rightarrow \pi^*)_{aromatic\ ring}$
	264	0.0172	4.686	(73 ->78), 0.41844	$(\pi \rightarrow \pi^*)_{aromatic\ ring}$
	367	0.584	3.372	(75 ->79) 0.33796,	$(\pi \rightarrow \pi^*)_{C=N}$
	415	0.0936	2.983	(76 ->79) 0.50111n (77 ->79) 0.70013 (77 ->78) 0.70130	$(n \rightarrow \pi^*)_{C=N}$
CHCl₃	257	0.0151	4.811	(73 ->79), 0.27768,	$(\pi \rightarrow \pi^*)_{aromatic\ ring}$
	264	0.0938	4.683	(73 ->78), 0.5644,	$(\pi \rightarrow \pi^*)_{aromatic\ ring}$
	364	0.589	3.040	(75 ->79), 0.20658	$(\pi \rightarrow \pi^*)_{C=N}$
	411	0.0946	3.012	(74 ->78) 0.36979, (74 ->79) 0.27698 (77 ->79) 0.70180 (77 ->78) 0.70326	$(n \rightarrow \pi^*)_{C=N}$
n-Hexane	254	0.0171	4.873	(76 ->79), 0.53489	$(\pi \rightarrow \pi^*)_{aromatic\ ring}$
	264	0.0037	4.695	(75 ->78) 0.43658,	$(\pi \rightarrow \pi^*)_{aromatic\ ring}$
	353	0.576	3.507	(74 ->78) 0.30784,	$(\pi \rightarrow \pi^*)_{C=N}$
	400	0.0950	3.096	(73 ->78) 0.34439, (73 ->79) 0.21030 (77 ->79) 0.69969 (77 ->78) 0.70293	$(n \rightarrow \pi^*)_{C=N}$
(2)					
Methanol	274	0.0870	4.525	(72 ->83), 0.24785,	$(\pi \rightarrow \pi^*)_{aromatic\ ring}$
	305	0.2046	4.055	(72 ->84), 0.36449,	$(\pi \rightarrow \pi^*)_{C=N}$
	467	0.1238	2.653	(78 -> 83), 0.40988 (82 ->85), 0.56559 (82 ->83), 0.70432	$(n \rightarrow \pi^*)_{C=N}$
Ethanol	274	0.0817	4.523	(72 ->83), 0.25448,	$(\pi \rightarrow \pi^*)_{aromatic\ ring}$
	305	0.2037	4.055	(72 ->84), 0.37694,	$(\pi \rightarrow \pi^*)_{C=N}$
	467	0.1275	2.653	(78 ->83), 0.39531 (80 ->84), 0.47100, (82 ->85), 0.28635 (82 ->83), 0.70432	$(n \rightarrow \pi^*)_{C=N}$
	DMSO	274	0.1234	4.519	(72 ->83), 0.20858,
306,		0.2058	4.048	(78 ->84), 0.48644	$(\pi \rightarrow \pi^*)_{C=N}$
468		0.1295	2.645	(80 ->84), 0.35120, (82 ->85), 0.56829 (82 ->83), 0.70422	$(n \rightarrow \pi^*)_{C=N}$
CH₂Cl₂		275	0.0110	4.500	(73 ->83), 0.26312,
	304	0.1684	4.078	(73 ->84), 0.51304	$(\pi \rightarrow \pi^*)_{C=N}$
	462	0.1524	2.682	(82 ->85), 0.57893 (82 ->83), 0.7036	$(n \rightarrow \pi^*)_{C=N}$
CHCl₃	274	0.0301	4.516	(73 ->83), 0.27439,	$(\pi \rightarrow \pi^*)_{aromatic\ ring}$
	305	0.1925	4.064	(73 ->84), 0.47440	$(\pi \rightarrow \pi^*)_{C=N}$
	465	0.1404	2.664	(82 ->85), 0.57939 (82 ->83), 0.70439	$(n \rightarrow \pi^*)_{C=N}$
n-Hexane	278	0.0092	4.457	(73 ->84), 0.49401	$(\pi \rightarrow \pi^*)_{aromatic\ ring}$
	303	0.1467	4.091	(82 ->85), 0.46224	$(\pi \rightarrow \pi^*)_{C=N}$
	452	0.1719	2.742	(82 ->83), 0.70134	$(n \rightarrow \pi^*)_{C=N}$

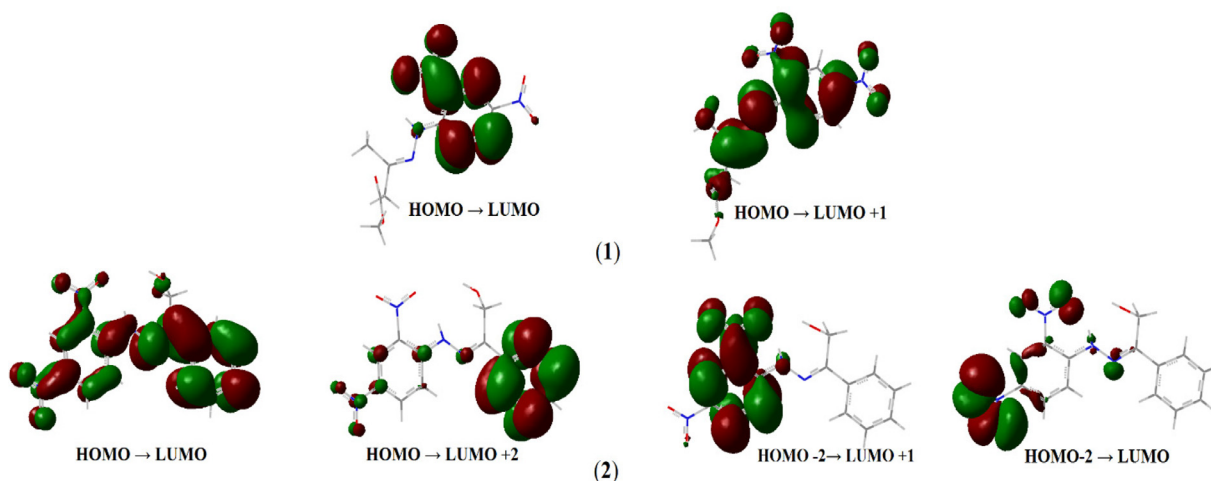


Fig. 5. The molecular orbital plots for (1) and (2).

Table 7

Calculated excitation wavelengths ($\lambda_{\text{cal}}/\text{nm}$), major contribution and energy of ligands in ethanol solvent.

Transition	λ_{cal}	Major contribution (>5%)	orbital distribution	Energy (eV)
(1)				
HOMO \rightarrow LUMO +1	369	97%	phenyl ring, C=N, N-H, (NO ₂) _{para, ortho} C=O and (CH ₃) _{Ketone} atoms	3.356
HOMO \rightarrow LUMO	418	97%	phenyl ring and (NO ₂) _{ortho} atoms	2.916
(2)				
HOMO \rightarrow LUMO+2, HOMO-2 \rightarrow LUMO+1, HOMO-2 \rightarrow LUMO	305	97.0%	phenyl ring, C=N and (NO ₂) _{ortho}	4.055
HOMO \rightarrow LUMO	467	99%	phenyl ring, N-H, C=N, (O) _{OH} and (NO ₂) _{Para, Ortho} atoms	2.653

through their interaction with the dissolved molecule. Investigations on compounds (1) and (2) showed that of the solvent effect is not significant. For the compound (1), the data obtained from TD-DFT in n-Hexane were more consistent with the experimental data. For the compound (2), the wavelengths in the polar solvent were similar to the non-polar solvent. More information on the calculated electronic spectroscopy data of compounds (1) and (2) are presented in Table 6.

3.4.4. Frontier molecular orbital analysis

According to the frontier molecular orbital theory, HOMO and LUMO are the most effective factors in the bioactivity. HOMO has the priority to provide electrons, while LUMO can accept electrons. Thus, the study on the frontier orbital energy can provide useful information about the biological mechanism. Also, The difference in energy between these two frontier orbitals can be used to predict the strength and stability of transition metal complexes, as well as the colors they produce in solution [38].

Fig. 5 displays the molecular orbital of compounds while Table 7 lists the calculated excitation wavelengths ($\lambda_{\text{cal}}/\text{nm}$) and energy of compounds. The HOMO and LUMO are scattered on phenyl ring atoms, C=N, NO₂, and N-H through various relations. In HOMO \rightarrow LUMO, the orbital distribution is larger on the phenyl ring and (NO₂)_{ortho} atoms. For HOMO \rightarrow LUMO +1 transitions (97% Occupied volume of orbitals), the orbital distribution was larger on the phenyl ring, C=N, N-H, (NO₂)_{para, ortho} C=O and (CH₃)_{Ketone} atoms of (1). In the case of (2), HOMO \rightarrow LUMO orbital distribution is largely distributed on the phenyl ring, N-H, C=N, (O)_{OH} and (NO₂)_{Para, Ortho} atoms; while in HOMO \rightarrow LUMO +2 (65%), the orbital distribution mainly on the (phenyl ring)_{Ketone}. For HOMO -2 \rightarrow LUMO +1 (25%), the orbital distribution is larger on

the (phenyl ring)_{hydrazine} and (NO₂)_{ortho} atoms whereas, in HOMO-2 \rightarrow LUMO (5%) of (2), the orbital distribution is larger on the (NO₂)_{para, ortho} atoms [25].

The electronic spectra show the energies of compounds (1) and (2) as 3.355 and 4.055 eV at the wavelengths of 369 and 305 nm, respectively. These high energy gaps indicate a good consistency as well as high chemical strength lower reactivity of the unit [39]. The compound (2) had the highest energy gap and higher chemical rigidity as compared with the compound (1).

3.5. Biological essays

3.5.1. Assessment of cytotoxicity using MTT assay

To further understanding on the mechanism of antiproliferative activities of hydrazine, their inhibitory activities for CDK4, CDK2, cyclin D, cyclin E proteins, and EGFR/ErbB-2 have been assessed. Most anticancer drugs are focused on blocking the cell cycle in the S or G2/M phases. It is well known that cisplatin usually induces cell cycle arrest at the S phase, which signifies the inhibition of DNA synthesis. The cell cycle distribution analysis of hydrazine and their complexes showed that they could markedly increase the cell death in S-phase or accumulation of the G1 population and induce cell apoptosis by cyclin D1/CDK4 inhibitory activity and DNA damage [40–42]. Moreover, hydrazines have demonstrated a potent dual inhibitory effect on EGFR/ErbB-2 as well as inhibiting ErbB-2 over-expressing in human cancer cell lines [43].

In another research, Shp2 (a protein tyrosine phosphatase (PTP) (PTPN11)) was inhibited by hydrazine (phenylhydrazonopyrazolone sulfonate) indicating that hydrazine can positively regulate the growth factor signaling in pediatric leukemia, juvenile myelomonocytic leukemia (JMML), and in myelodysplastic syndrome, acute

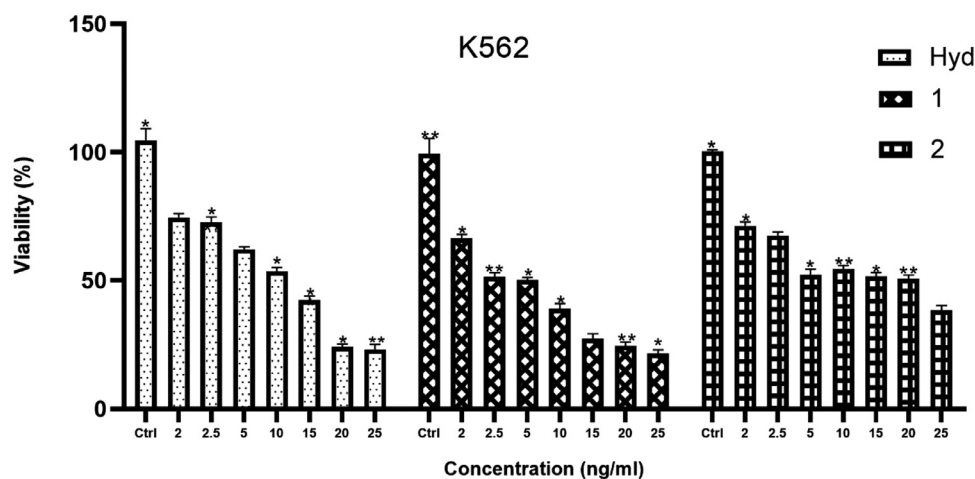


Fig. 6. The anti-growth effect after the treatment with varying doses of compounds 2, 4-dinitrophenylhydrazine, (1) and (2), against cancer cell line in K562 (myelogenous leukemia cancer) by the MTT as described in the experimental section. Data were normalized as a percentage of values of the control ($p < 0.05$).

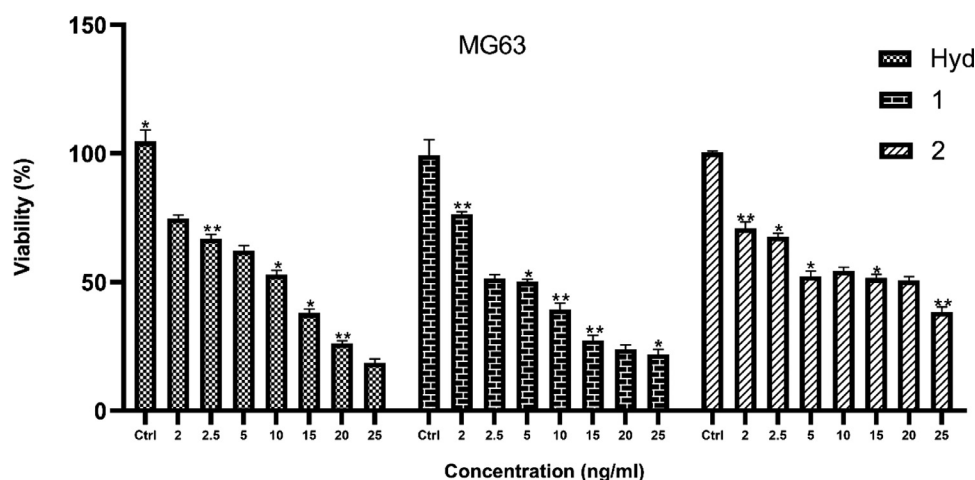


Fig. 7. The anti-growth effect after the treatment with varying doses of compounds 2, 4-dinitrophenylhydrazine, (1) and (2), against cancer cell line in MG63 (osteosarcoma cancer) by the MTT as described in the experimental section. Data were normalized as a percentage of values of the control ($p < 0.05$).

myeloid leukemia, and some solid tumors [44]. Furthermore, sulfonylhydrazone has been considered as a potent Phosphatidylinositol 3-kinase (PI3K) inhibitor. As a regulator of intracellular signaling pathways, PI3K signaling can be negatively regulated by PTEN, which is overexpressed in the majority of human cancers as one of the most commonly mutated proteins [45, 46]. N-benzoxazol-2-yl-N'-1-(isoquinolin-3-yl-ethylidene)-hydrazine (EPH136) has shown antitumor activity by DNA synthesis, RNA synthesis, and ribonucleotide reductase [47]. Cell cytotoxicity of aroylhydrazone complexes Ln(III) was examined by a standard MTT assay on hepatoblastoma cells (HepG2) and human lung adenocarcinoma epithelial cells (A549). These results suggested high anti-tumor activity of the Ln(III) complexes through the necrotic mechanism and DNA cleavage [48]. The MTT assay is a suitable approach to assess the *in vitro* anticancer activity of the compounds. It is expressed as the required concentration of compounds for 50% inhibition of cancer cell viability (IC_{50}) after 48 h [49–51].

The synthesized compounds were screened for their *in vitro* cytotoxicity and growth inhibitory activities against different human tumor cell lines including myelogenous leukemia cancer K562 and osteosarcoma cancer MG63. 5-Fluorouracil is a common drug used to treat gastric and colorectal cancers. The 5-Fluorouracil-treated cells treated were considered positive control; while the untreated ones were regarded as negative control [52]. As shown in Figs. 6 and 7, IC_{50} values of 2, 4-dinitrophenylhydrazine (1) and (2) were

dose-dependent against K562 and MG63 cell lines with approximate IC_{50} values of 10, 2.5 and 5 ng/mL at 48 h, respectively. Consequently, it has been suggested that the newly synthesized compounds (1) and (2), showed anticancer activity toward K562 and MG63 cell lines. Detailed *in vivo* and *in vivo* tests of anticancer efficacy of these compounds must be surveyed in the future. Moreover, the compound (1) exhibits the highest cytotoxic activity.

In this study, the Schiff's base hydrazine derivatives were synthesized from methyl acetoacetate and α -hydroxyacetophenone with 2, 4-dinitrophenylhydrazine. The structures of the compounds (1) and (2) were investigated by X-ray diffraction. Also, FT-IR, UV-Vis, 1H NMR, Mass spectra, melting point assessments, and conductivity measurements were conducted for sample characterization. DFT calculations were used to study the optimized structure of these ligands as well as their FT-IR, and UV-Vis spectra. The spectroscopic data concerning compounds in the "Experimental" section are in good agreement with the expected values. The anticancer effects of the compounds were evaluated towards K562 and MG63 using MTT assay. The synthesized compounds were screened for dose-dependent *in vitro* anticancer activities against myelogenous leukemia cancer K562 and osteosarcoma cancer MG63. Comparing the IC_{50} values revealed that both compounds (1) and (2) had high cytotoxic activity against the K562 and MG63 cancer cells. These results suggest that compounds (1) and (2) may be

considered as a therapeutic agent in cancer treatment and management.

Author contribution statement

SP. conducted most of the experiments. SP, analyzed the data with the help of MS and prepared the manuscript under the supervision of MS. MS directed, designed, gave insight and interpreted the spectroscopic data of the research project. AG. carried out the X-ray analysis of this project. AK. did the Biological study of this project. All authors have significant contribution on conducting this research work and presenting the manuscript.

Declaration of Competing Interest

The authors declare that they have no known competing financial interests or personal relationships that could have appeared to influence the work reported in this paper.

Acknowledgments

We thank Semnan University for supporting this study. The authors deem it necessary to appreciate Mrs. Anita Grześkiewicz, Adam Mickiewicz University, Poznan, Poland, Mr. Ali Khaleghian, Biochemistry Department, University of Medical Sciences, Semnan, Iran, who generously helped us to flourish this research work.

Supplementary materials

Supplementary material associated with this article can be found, in the online version, at [doi:10.1016/j.molstruc.2020.129086](https://doi.org/10.1016/j.molstruc.2020.129086).

References

- [1] M. Masoudi, M. Behzad, A. Arab, A. Tarahhomi, H. Amiri Rudbari, G. Bruno, Crystal structures, DFT calculations and Hirshfeld surface analyses of three new cobalt(III) Schiff base complexes derived from meso-1, 2-diphenyl-1, 2-ethylenediamine, *J. M. Struct.* 1122 (2016) 123–133.
- [2] S.T. Tsantis, D.I. Tzimopoulos, M. Holynska, S.P. Perlepes, Oligonuclear actinoid complexes with Schiff bases as ligands—older achievements and recent progress, *Int. J. Mol. Sci.* 21 (2020) 555.
- [3] X. Liu, J.R. Hamon, Recent developments in penta-, hexa- and heptadentate Schiff base ligands and their metal complexes, *Coord. Chem. Rev.* 389 (2019) 94–118.
- [4] L. Rigamonti, A. Forni, S. Righetto, A. Pasini, Push–pull unsymmetrical substitution in nickel(II) complexes with tetradentate N_2O_2 Schiff base ligands: synthesis, structures and linear–nonlinear optical studies, *Dalton Trans* 48 (2019) 11217–11234.
- [5] Z.M. Almarhoon, W.A. Al-Onazi, A.A. Allothman, A.M. Al-Mohaimed, E.S. Al-Farraj, Synthesis, DNA binding, and molecular docking studies of dimethylaminobenzaldehyde-based bioactive Schiff bases, *J. Chem.* (2019) 1–14.
- [6] J.E. Baumeister, K.M. Reinig, C.L. Barnes, S.P. Kelley, S.S. Jurisson, Technetium and Rhenium Schiff base compounds for nuclear medicine: syntheses of Rhenium analogues to ^{99m}Tc -Furifosmin, *Inorg. Chem.* 57 (2018) 12920–12933.
- [7] H. Ji, H. Ni, P. Zhi, Z. Xi, W. Wang, J. Shi, Y. Shen, Visible-light mediated directed perfluoroalkylation of hydrazones, *Org. Biomol. Chem.* 15 (2017) 6014–6023.
- [8] G. Le Goff, Natural hydrazine-containing compounds, Biosynthesis, isolation, biological activities and synthesis, *J. Ouazzani, Bioorg. Med. Chem.* 22 (2014) 6529.
- [9] V. Onnis, M.T. Cocco, R. Fadda, C. Congiu, Synthesis and evaluation of anticancer activity of 2-arylamino-6-trifluoromethyl-3-(hydrazonocarbonyl)pyridines, *Bioorg. Med. Chem.* 17 (2009) 6158–6165.
- [10] N. Filipovic, H. Borrmann, T. Todorovic, M. Borna, V. Spasojevic, D. Sladic, I. Novakovic, K. Andjelkovic, Copper(II) complexes of N-heteroaromatic hydrazones: synthesis, X-ray structure, magnetic behavior, and antibacterial activity, *Inorg. Chim. Acta.* 362 (2009) 1996–2000.
- [11] M.C. Rodríguez-Argüelles, R. Cao, A.M. García-Deibe, C. Pelizzi, J. Sanmartín-Matalobos, F. Zani, Antibacterial and antifungal activity of metal(II) complexes of acylhydrazones of 3-isatin and 3-(N-methyl)isatin, *Polyhedron* 28 (2009) 2187–2195.
- [12] M. Milenković, A. Pevec, I. Turel, M. Vujčić, M. Milenković, K. Jovanović, N. Gligorijević, S. Radulović, M. Swart, M. Gruden-Pavlović, K. Adaila, B. Cobeljčić, K. Andelković, Synthesis, characterization, DFT calculation and biological activity of square-planar Ni(II) complexes with tridentate PNO ligands and monodentate pseudohalides. Part II, *Eur. J. Medicinal Chem.* 87 (2014) 284e297.
- [13] H.H. Eissa, Synthesis, characterization, anticorrosion activity and antibacterial activity of macrocyclic schiff bases based on 1, 3-dithiocarbonyl phenyl dihydrazide, *Organic Chem Curr Res* 4 (2015) 151.
- [14] P.G. Avaji, C.H. Kumar, S.A. Patil, K.N. Shivananda, C. Nagaraju, Synthesis, spectral characterization, in-vitro microbiological evaluation and cytotoxic activities of novel macrocyclic bis hydrazone, *Eur. J. Med. Chem.* 44 (9) (2009) 3552–3559.
- [15] R. Lazny, A. Nodzevska, N. N-dialkylhydrazones in organic synthesis. From simple N, N-dimethylhydrazones to supported chiral auxiliaries, *Chem. Rev.* 110 (2010) 1386.
- [16] S.K. Bharti, G. Nath, R. Tilak, S.K. Singh, Synthesis, anti-bacterial and anti-fungal activities of some novel Schiff bases containing 2, 4-disubstituted thiazole ring, *Eur. J. Medicinal Chem.* 45 (2010) 651–660.
- [17] S.N. Podyachev, B.M. Gabidullin, V.V. Syakaev, S.N. Sudakov, A.T. Gubaidullin, W.D. Habicher, A.I. Konovalov, The role of preorganization of hydrazone moieties on tetrathiacalix[4]arene platform for their conformational and binding properties from the view of structural investigation, *J. Mol. Struct.* 1001 (2011) 125–133.
- [18] Z.H. Chohan, M.A. Farooq, A. Scozzafava, C.T. Supuran, Antibacterial Schiff bases of oxalyl-hydrazine/diamide incorporating pyrrolyl and salicylyl moieties and of their zinc(II) complexes, *J. Enzyme Inhib. Med. Chem.* 17 (1) (2002) 1–7.
- [19] P. Crisalli, E.T. Kool, Importance of ortho proton donors in catalysis of hydrazone formation, *Org. Lett.* 15 (7) (2013) 1646–1649.
- [20] W.-L. Ye, Y.-P. Zhao, H.-Q. Li, R. Na, F. Li, Q.-B. Mei, M.-G. Zhao, S.-Y. Zhou, Doxorubicin-poly (ethylene glycol)-alendronate self-assembled micelles for targeted therapy of bone metastatic cancer, *Sci. Rep.* 5 (2015) 14614.
- [21] H.H. Monfared, O. Pouralimardan, C. Janiak, Synthesis and spectral characterization of hydrazone Schiff bases derived from 2, 4-dinitrophenylhydrazine. crystal structure of salicylaldehyde-2, 4-dinitrophenylhydrazone, *Z. Naturforschung* 62 (5) (2007) 717–720 B.
- [22] Ji. Ning-Ning, Shi Zhi-Qiang, 1-Cyclopentylidene-2-(2, 4 dinitrophenyl)-hydrazine, *Acta Cryst* 64 (2008) o2141 E.
- [23] Ji. Ning-Ning, Shi. Zhi-Qiang Shi, Zhao Ren-Gao, Zheng Ze-Bao, Li. Zhi-Feng, Synthesis, crystal structure and quantum chemistry of a novel Schiff base N-(2, 4-dinitro-phenyl)-N'-(1-phenyl-ethylidene)-hydrazine, *Bull. Korean Chem. Soc.* 31 (2010) 4.
- [24] H. Hongfei, L. Yaohua, A monoclinic polymorph with Z = 4 of (E)-2, 4-dihydroxyacetophenone 2, 4-dinitrophenylhydrazone N, Ndimethylformamide monosolvate, *Acta Cryst.* (2011).
- [25] S. Parvarinezhad, M. Salehi, Sh. Kademia, M. Kubicki, The structural study, Hirshfeld surface analysis, and DFT calculations of ferrocenyl-hydrazine Schiff base: a novel precursor for the selective preparation of Fe_2O_3 nanoparticles, *J. Mol. Struct.* 1197 (2019) 96–107.
- [26] W.J. Geary, The use of conductivity measurements in organic solvents for the characterisation of coordination compounds, *Coord. Chem. Rev.* 253 (1997) 81–122.
- [27] Agilent Technologies, CrysAlis PRO (Version 1.171.33.36d), Agilent Technologies Ltd, 2011.
- [28] G.M. Sheldrick, Synthesis, characterization and crystal structure of a new schiff base ligand from a bis (thiazoline) template and hydrolytic cleavage of the imine bond induced by a Co(II) cation, *Acta Crystallogr.* 71 (2015) 3–8 C.
- [29] A.D. Becke, Density-functional exchange-energy approximation with correct asymptotic behavior, *Phys. Rev.* 38 (1988) 3098.
- [30] C. Lee, W. Yang, R.G. Parr, Development of the Colle-Salvetti correlation-energy formula into a functional of the electron density, *Phys. Rev. B Condens. Matter.* 37 (1988) 785.
- [31] A.D. Becke, Density-functional thermochemistry. III. The role of exact exchange, *J. Chem. Phys.* 98 (1993) 5648.
- [32] C. Lee, W. Yang, R.G. Parr, Development of the Colle-Salvetti correlation-energy formula into a functional of the electron density, *Phys. Rev.* 37 (1988) 785 B.
- [33] M.J. Frisch, G.W. Trucks, H.B. Schlegel, G.E. Scuseria, M.A. Robb, J.R. Cheeseman, J.A. Montgomery Jr., T. Vreven, K.N. Kudin, J.C. Burant, J.M. Millam, S.S. Iyengar, J. Tomasi, V. Barone, B. Mennucci, M. Cossi, G. Scalmani, N. Rega, G.A. Petersson, H. Nakatsuji, M. Hada, M. Ehara, K. Toyota, R. Fukuda, J. Hasegawa, M. Ishida, T. Nakajima, Y. Honda, O. Kitao, H. Nakai, M. Klene, X. Li, J.E. Knox, H.P. Hratchian, J.B. Cross, C. Adamo, J. Jaramillo, R. Gomperts, R.E. Stratmann, O. Yazyev, A.J. Austin, R. Cammi, C. Pomelli, J.W. Ochterski, P.Y. Ayala, K. Morokuma, G.A. Voth, P. Salvador, J.J. Dannenberg, V.G. Zakrzewski, S. Dapprich, A.D. Daniels, M.C. Strain, O. Farkas, D.K. Malick, A.D. Rabuck, K. Raghavachari, J.B. Foresman, J.V. Ortiz, Q. Cui, A.G. Baboul, S. Clifford, J. Cioslowski, B.B. Stefanov, G. Liu, A. Liashenko, P. Piskorz, I. Komaromi, R.L. Martin, D.J. Fox, T. Keith, M.A. Al-Laham, C.Y. Peng, A. Nanayakkara, M. Challacombe, P.M.W. Gill, B. Johnson, W. Chen, M.W. Wong, C. Gonzalez, J.A. Pople, Gaussian 09 (Linux Version), 2009.
- [34] V. Selvarani, B. Annaraj, M.A. Neelakantana, S. Sundaramoorthy, D. Velmurgan, Synthesis and crystal structure of hydroxyacetophenone Schiff bases containing propargyl moiety: solvent effects on UV-visible spectra, *Spectrochimica Acta Part A* 91 (2012) 329–337.
- [35] E.A. Dikumar, V.I. Potkin, Synthesis and Properties of Substituted Benzaldehyde Phenylhydrazones, *Rus. J. Gener. Chem.* 5 (2009) 953–956.
- [36] A. Gavezzotti, Are crystal structures predictable, *Acc. Chem. Res.* 27 (1994) 309–314.
- [37] A. Gavezzotti, G. Filippini, Geometry of the intermolecular X-H...O hydrogen bond and the calibration of empirical hydrogen-bond potentials, *J. Phys. Chem.* 98 (1994) 4831–4837.

- [38] J.-X. Mu, M.-Y. Yang, Z.-H. Sun, C.-X. Tan, J.-Q. Weng, H.-K. Wu, X.-H. Liu, Synthesis, crystal structure and DFT Studies of 8-chloro-3-((3-chlorobenzyl)thio)-[1, 2, 4]triazolo[4, 3-a]pyridine, *Crystals* 5 (2015) 491–500.
- [39] A. Arab, F. Gobal, N. Nahali, M. Nahali, Electronic and structural properties of neutral, anionic, and cationic $Rh \times Cu_4x$ ($x = \frac{1}{4}, 0e4$) small clusters: a DFT study, *J. Clust. Sci.* 24 (2013) 273.
- [40] X.Q. Song, Zh.G Wang, Y. Wang, Y.Y. Huang, Y.X. Suna, Y. Ouyang, Ch.Zh Xie, J.Y. Xu, Syntheses, characterization, DNA/HSA binding ability, and antitumor activities of a family of isostructural binuclear lanthanide complexes containing hydrazine Schiff base, *J. Biomol. Struct. Dyn.* (2019), doi:10.1080/07391102.2019.1587511.
- [41] T. Horiuchi, J. Chiba, K. Uoto, T. Soga, Discovery of novel thieno[2, 3-d]pyrimidin-4-yl hydrazone-based inhibitors of Cyclin D1-CDK4: synthesis, biological evaluation, and structure–activity relationships, *Bioorg. Med. Chem. Lett.* 19 (2009) 305–308.
- [42] T. Horiuchi, M. Nagata, M. Kitagawa, K. Akahane, K. Uoto, Discovery of novel thieno[2, 3-d]pyrimidin-4-yl hydrazone-based inhibitors of Cyclin D1-CDK4: synthesis, biological evaluation and structure–activity relationships. Part 2, *Bioorg. Med. Chem.* 17 (2009) 7850–7860.
- [43] G. Xu, M.C. Abad, P.J. Connolly, M.P. Neeper, G.T. Struble, B.A. Springer, S.L. Emanuel, N. Pandey, R.H. Gruninger, M. Adams, S. Moreno-Mazza, A.R. Fuentes-Pesquera, S.A. Middleton, 4-Amino-6-aryl-amino-pyrimidine-5-carbaldehyde hydrazones as potent ErbB-2/EGFR dual kinase inhibitors, *Bioorg. Med. Chem.* 18 (2008) 4615–4619.
- [44] K. Hellmuth, S. Grosskopf, C.T. Lum, M. Wörtele, N. Röder, J.P. von Kries, M. Rosario, J. Rademann, W. Birchmeier, Specific inhibitors of the protein tyrosine phosphatase Shp2 identified by high-throughput docking, *PANS* 105 (2008) 7275–7280.
- [45] M. Hayakawa, K.I. Kawaguchi, H. Kaizawa, T. Koizumi, T. Ohishi, M. Yamano, M. Okada, M. Ohta, Sh.I. Tsukamoto, F.I. Raynaud, P. Parker, P. Workman, M.D. Waterfield, Synthesis and biological evaluation of sulfonylhydrazonesubstituted imidazo[1, 2- α]pyridines as novel PI3 kinase p110 α inhibitors, *Bioorg. Med. Chem.* 15 (2007) 5837–5844.
- [46] G.R. Gao, J.L. Liu, D. Sh. Mei, J. Ding, L.H. Meng, W.H. Duan, Design, synthesis and biological evaluation of acylhydrazones derivatives as PI3K inhibitors, *Chin. Chem. Lett.* 26 (2015) 118–120.
- [47] J. Hofmann, J. Easmon, G. Puerstinger, G. Heinisch, M. Jenny, A.A. Shtil, M. Hermann, D.F. Condorelli, S. Sciré, G. Musumarra, N-benzoxazol-2-yl-N'-1-(isoquinolin-3-yl-ethylidene)-hydrazine, a novel compound with antitumor activity, induces radicals and dissipation of mitochondrial membrane potential, *Invest New Drugs* 27 (2009) 189–202.
- [48] X.-Q. Song, -G. Wang Zh, Y. Wang, -Y. Huang Y, -X. Sun Y, Y. Ouyang, -Zh Xie Ch, J.-Y. X. u, Syntheses, characterization, DNA/HSA binding ability, and antitumor activities of a family of isostructural binuclear lanthanide complexes containing hydrazine Schiff base, *Biomol. Struct. Dyn.* (2018).
- [49] R.E. Malekshah, M. Salehi, M. Kubicki, A. Khaleghian, Crystal structure, molecular docking, and biological activity of the zinc complexes with 2-thenoyltrifluoroacetone and N-donor heterocyclic ligands, *J. Mol. Struct.* 155 (2017) 1150.
- [50] R.E. Malekshah, M. Salehi, M. Kubicki, A. Khaleghian, New mononuclear copper(II) complexes from β -diketone and β -keto ester N-donor heterocyclic ligands: structure, bioactivity, and molecular simulation studies, *J. Coord. Chem.* 71 (2018) 952–968.
- [51] R.E. Malekshah, M. Salehi, M. Kubicki, A. Khaleghian, Biological studies and computational modeling of two new copper complexes derived from β -diketones and their nano-complexes, *J. Coord. Chem.* 72 (2019) 1697–1714.
- [52] Z. Abbasi, M. Salehi, M. Kubicki, A. Khaleghian, Crystal structures, electrochemical properties, antioxidant screening and in vitro cytotoxic studies on four novel Cu(II) complexes of bidentate Schiff base ligands derived from 2-methoxyethylamine, *J. Coord. Chem.* 70 (2017) 2074–2093.